# High frequency sheath modulation and higher harmonic generation in a low pressure very high frequency capacitively coupled plasma excited by sawtooth waveform

Sarveshwar Sharma[1,2], Nishant Sirse[3] and Miles M Turner[4]

[1]Institute for Plasma Research, Gandhinagar – 382428, India

[2]Homi Bhabha National Institute, Anushaktinagar, Mumbai – 400094, India

[3]Institute of Science & Laboratory Education, IPS Academy, Indore -452012, India

[4]School of Physical Sciences and National Center for Plasma Science and Technology, Dublin City University, Dublin 9, Ireland

E-mail: nishantsirse@ipsacademy.org

**Abstract**

A particle-in-cell (PIC) simulation study is performed to investigate the discharge asymmetry, higher harmonic generations and electron heating mechanism in a low pressure capacitively coupled plasma (CCP) excited by a saw-tooth like current waveform for different driving frequencies; 13.56 MHz, 27.12 MHz, and 54.24 MHz. Two current densities, 50 A/m$^2$ and 100 A/m$^2$ are chosen for a constant gas pressure of 5 mTorr in argon plasma. At a lower driving frequency, high frequency modulations on the instantaneous sheath electric field near to the grounded electrode are observed. These high frequency oscillations create multiple ionization beam like structures near to the sheath edge that drives the plasma density in the discharge and responsible for discharge/ionization asymmetry at lower driving frequency. Conversely, the electrode voltage shows higher harmonics generation at higher driving frequencies and corresponding electric field transients are observed into the bulk plasma. At lower driving frequency, the electron heating is maximum near to the sheath edge followed by electron cooling within plasma bulk, however, alternate heating and cooling *i.e.* burst like structures are obtained at higher driving frequencies. These results suggest that electron heating in these discharges will not be described accurately by simple analytical models.

## 1. Introduction

Capacitively coupled plasmas (CCP's) are one of the most fundamental etching tools used in the semiconductor industries for the fabrication of large-scale integrated circuits [1]. An independent control of ion flux and mean ion energy is vital for plasma etching and it was first made achievable by using a dual-frequency (DF) voltage waveform applied on the same electrode [2]. In such discharges, the high-frequency voltage amplitude controls the ion flux as it drives plasma density in the discharge. Whereas, the ion impact energy on the substrate is controlled by the low-frequency voltage amplitude. Several simulation and experimental studies [3-8] were reported to understand the behavior of DF CCP's under different operating conditions. It was observed that both low and high frequency coupling, and secondary electron emission from the electrodes can affect the independent control of ion flux and ion energy in DF CCP's [9-10]. In one of the research findings, it was reported that *ion energy distribution function* (IEDF) can be controlled by imposing an intermediate frequency in DF-CCPs [11]. In this type of triple frequency excited CCP configuration, the effect of intermediate frequency on plasma parameters has been studied by various numerical simulation techniques [11-15]. The other novel technique, Electrical Asymmetric Effect (EAE) was proposed to control the ion properties, introduced by Heil *et al.* [16-17]. In this technique, the plasma was excited with the help of a fundamental frequency and its second harmonic that lead to the formation of a DC self-bias even in geometrically symmetrical CCP discharges. The phase between the two harmonics can control the self-bias that can directly affect the energy of the ions at the electrodes without affecting the ion flux [18]. The implementation of the EAE has been thoroughly examined in both electropositive and electronegative plasmas comprising different physical mechanisms like power absorption by electrons, effect of the secondary electron emission and driving frequencies [19-22]. Asymmetry effect and DC self-bias could also be generated by manipulating several other factors such as the different electrode sizes knows as "geometrical asymmetry" [23-25] or by choosing electrodes of differing materials known as "secondary electron asymmetry effect" [26].

In a recent development, the excitation of capacitively coupled radio-frequency discharges using tailored waveform has emerged as a promising tool for an effective control of ion flux and ion energy in technological plasmas [27]. These tailored waveforms are also known as customized waveforms, which have non-sinusoidal shape [28-34] and can be generated by superimposition of signal with a fundamental frequency and its higher harmonics with an appropriate phase shift between them. The shape of the waveform can be modified by changing the harmonics amplitude and their phases. In recent years, tailored waveforms played an important role in silicon etching [35-36] and thin film deposition [37-38]. More specifically, a novel type of temporally asymmetric waveform known as sawtooth waveform, which is the family of tailored waveform was introduced by Bruneau *et al.*

[39-41]. It consists of a fast rise and slow fall or vice versa that has slope asymmetry but no amplitude asymmetry. The amplitude asymmetry has been comprehensively examined for dual-frequency excitation [42-45] and for the waveforms including more harmonics [46-51]. Using Phase resolved optical emission spectroscopy (PROES), a strong ionization asymmetry was observed in a voltage driven CCP excited by an ideal sawtooth-like waveform that contains higher number of harmonics [41].

The work of Bruneau *et al.* [39] reported the effect of sawtooth voltage waveform with different rise and fall slopes. They performed PIC simulation in argon gas with a discharge gap of 2.5 cm, 13.56 MHz applied frequency, neutral gas pressure of 400 mTorr, 200 V peak to peak applied voltage and the secondary electron emission was considered in their study. Their results showed that the fast sheath expansion adjacent to powered electrode triggers an enormous pressure heating, which results a high ionization rate near to the sheath edge. On the other hand, gradual sheath expansion near to the grounded electrode results in weak heating and a low ionization rate. Subsequently, a large ion flux ($\Gamma_i$) asymmetry develops with a lower flux reaching on the grounded electrode. Furthermore, depending on the shape of the applied sawtooth voltage waveform *i.e.* sawtooth-up or sawtooth-down one can switch from a positive to negative self-bias respectively. Later in 2015, Bruneau *et al.* [40] extended their previous work for the same set of simulation parameters as described above. The effect of pressure (20 mTorr to 800 mTorr) on discharge asymmetry was investigated at 200 V discharge voltage and 13.56 MHz applied frequency. The simulation outcome showed that at 20 mTorr, the ionization mainly occurs in the bulk plasma and no asymmetry was seen. The discharge shifts from bulk ionization to the sheath ionization as pressure increases and the asymmetry appears. As the pressure increase to 800 mTorr, the asymmetry becomes more intense because of the significant local ionization near to the sheath edge. Another important study reported in this paper is the effect of changing the base frequency (1.695 MHz, 3.39 MHz, 13.56 MHz and 54.24 MHz) at 400 mTorr gas pressure. It was shown that the time averaged ionization rate ($<K_{iz}>$) is strongly reduced when applied frequency ($f_{rf}$) is reduced *i.e.* it is maximum at 54.24 MHz and minimum at 1.695 MHz. It is noted that the maximum of $<K_{iz}>$ moves away from the powered electrode when $f_{rf}$ is decreased because of the larger sheath width. Their explanation was based on two opposing mechanisms. With decreasing $f_{rf}$, the asymmetric effect is lower and the ionization peak shifts away from the powered electrode because diffusion to the opposing electrode is facilitated. On the other side, when the local maxima close to the grounded electrode is lower the asymmetry is higher because the asymmetry of ion creation is increased. As a result, when $f_{rf}$ is reduced two mechanisms work, first one which increases the asymmetry and the other one which tends to decrease it. Therefore, the asymmetry behavior depends on the dominant effect. It was reported that density is strongly reduced when $f_{rf}$ is reduced from 54.24 to 3.39 MHz and the density profile is more and more asymmetric. This explains that the second mechanism as described above, *i.e.* the drop of ionization peak near to grounded electrode, plays the dominant role.

The previous study concerning the effect of base frequency of a sawtooth-like waveform on discharge asymmetry was performed in the high-pressure regime [40]. However, the applied frequency effect at a low gas pressure *i.e.* in the collisionless regime, which is typically the case in plasma processing was not reported in the literature. Furthermore, the electric field transients and higher harmonic generation in the discharge excited by the sawtooth-like waveform is never studied. These transients are generated at a very high frequency and for the collisionless case travel though the bulk plasma up to the opposite sheath. Depending on their energies these transients modify the instantaneous sheath edge position. In this manuscript, we show the effect of driving frequency in a nearly collisionless regime. The asymmetry effect is investigated along with the electric field transients, higher harmonic generations and electron heating mechanism. The simulation is performed for an ideal [41] saw-tooth current waveform (see figure 1) that contains a higher number of harmonics (see equation 1). Our simulation results showed high frequency modulation on the instantaneous sheath electric field near to the grounded electrode. Distinct higher harmonics are triggered that are observed in both electric field at the centre of the discharge and in the electrode voltage. Alternate heating and cooling *i.e.* burst like structures at higher driving frequencies suggest that the electron heating in such system is highly complex and can't be determined by simple analytical models [52-53].

The article is structured as follows. The simulation technique that is established on Particle-in-Cell/Monte Carlo collision (PIC/MCC) methods is described in section II. The physical interpretation and description of simulation results are presented in section III. In section IV, the summary and conclusion are given.

## 2. Simulation Technique and Parameters

A *current driven* symmetric capacitively coupled discharge in argon plasma is simulated here by using a well-tested and benchmarked 1D3V, electrostatic, self-consistent, particle-in-cell (PIC) code. The Particle-in-Cell/Monte Carlo collision (PIC/MCC) methods is the core of this simulation technique and its detail can be found in literature [54-55]. This code is developed at Dublin City University by Prof. Miles Turner and extensively used in several research articles and few of them can be find here [56-66]. This code can run in both current and voltage driven modes and we have opted for the current driven mode for the present paper. The details of the simulation technique are reported in literature [67-68]. In our simulation, we have considered all important particle particle collision reactions like ion-neutral (elastic, inelastic and charge exchange), electron-neutral (elastic, inelastic and ionization) and processes like multi-step ionization, metastable pooling, partial de-excitation, super elastic collisions and further de-excitation. The type of reactions and others details are given in the literature [58]. The creation of metastables (*i.e.* Ar*, Ar**) has been considered in simulation and also tracked them in our output diagnostics. These two lumped excited states of Ar, *i.e.*, Ar* ($3p^5 4s$), 11.6 eV, and Ar** ($3p^5 4p$), 13.1 eV, in

uniform neutral argon gas background is considered with charged particles viz. electrons and ions in simulation. The details of species included in simulation, their reactions and cross sections are taken from well-tested sources in the literature [58, 63, 69]. The stability and accuracy criterion of PIC is addressed by choosing appropriate grid size (Δx) and time step size (Δt) that can resolve the Debye length and the electron plasma frequency respectively. It is assumed that both the electrodes have infinite dimension and are planar and parallel to each other. We have also considered that electrodes are perfectly absorbing and for the sake of simplicity secondary electron emission is ignored. The discharge gap is 6 cm and is operated at a gas pressure of 5 mTorr. The gas is uniformly distributed with a fixed temperature 300 K. The temperature of ions is the same as the neutral gas. The number of particles per cell is 100 for all sets of simulation.

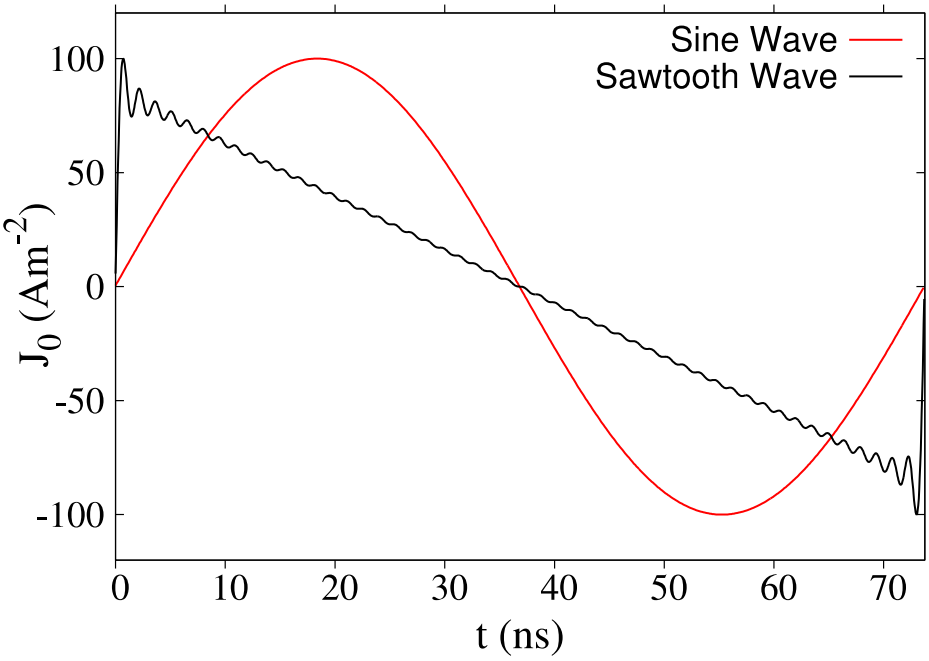


**Figure 1:** Profile of sinusoidal ($k$ = 1) and sawtooth ($k$ = 50) current waveform from equation (1) for 13.56 MHz and current density amplitude of 100 A/m$^2$.

A complex structure of applied waveform can be produced by employing an adequately high number of harmonics of a fundamental RF frequency. For current driven CCP, the sawtooth waveform has following expression (see figure 1):

$$J_{rf}(t) = \pm J_0 \sum_{k=1}^{N} \frac{1}{k} \sin(k\omega_{rf} t) \qquad \text{----------(1)}$$

where positive and negative signs correspond to “sawtooth-down” and “sawtooth-up” waveforms respectively. Here, $J_o$ is the current density amplitude applied at the

powered electrode, and $\omega_{rf}$ is the fundamental angular driven radiofrequency. The magnitude $J_0$ varies with the total number of harmonics *i.e.* N (which is 50 here) and is arranged in a way to provide the required peak-to-peak current density amplitude. Figure 1 shows the profile of sawtooth current waveform for N=50 case and the sinusoidal waveform w.r.t. time in nanosecond (ns). Here the chosen frequency is 13.56 MHz and current amplitude is 100 A/m$^2$. A higher value of N gives an ideal sawtooth profile. An expression similar to equation (1) for the voltage waveform case can be found in reference [41]. We have used "sawtooth-down" current waveform for all set of our simulations.

A choice of the current source is arbitrary as the principle motivation of the work is to study the effect of driving frequency on the non-linearity generated in the system when excited by a sawtooth-like waveform. Furthermore, for a current driven case, a direct comparison of the simulation results could be made with the analytical models as they consider mostly the constant current condition [52-53]. For the experiments, although rare, a current source can be obtained by implementing an RF amplifier or generator with a very high output impedance in comparison to the plasma impedance [70-71]. In this case, one can neglect the additional impedance of the plasma source and therefore current becomes the controlling parameter.

## 3. Results and Discussions

The velocity of energetic electrons produced from near to the sheath edge is affected by the shape of applied waveform and driving frequency *i.e.* it influences the sheath dynamics significantly and therefore the plasma profile changes drastically. Figure 2 (a) and 2 (b) shows the time average ion and electron density profile within discharge system at 13.56 MHz, 27.12 MHz and 54.24 MHz driving frequency for current density amplitudes of 50 A/m$^2$ and 100 A/m$^2$ respectively. In figure 2, the RF current source is applied at 0 cm and the grounded electrode is at 6 cm. Strong asymmetry is observed at lower driving frequencies. At 13.56 MHz and 50 A/m$^2$, the results showed that the sheath width near to the grounded electrode is broader (~ 10 mm) when compared to the sheath width near to powered electrode (~ 6 mm). The sheath width is estimated as where the electron sheath edge is at maximum distance from the electrode and quasi-neutrality breaks down. A sharp dip in the electron density is observed at this point when moving from bulk plasma towards electrode. When the applied frequency is increased from 13.56 MHz to 27.12 MHz, the sheath width near grounded and powered electrode are ~ 5 mm and ~4 mm respectively. The density profile is more symmetric compared to 13.56 MHz case. When the frequency is further increased to 54.24 MHz, the density profile is nearly symmetric and the sheath width near to the electrodes are approximately 3 mm. The asymmetry is accompanied by the DC self-bias that is generated at the powered electrode. At 50 A/m$^2$, the DC self-bias is ~210 V at 13.56 MHz and decrease to ~3 V at 54.24 MHz driving frequency. Similar asymmetry trend is observed at a current density of 100 A/m$^2$. The DC self-bias at 100 A/m$^2$ is ~470 V at 13.56 MHz and decrease to ~5 V at 54.24 MHz

driving frequency. Above description demonstrates that the asymmetry in the density profile can be controlled by changing the applied base frequency in the case of sawtooth-like waveform.

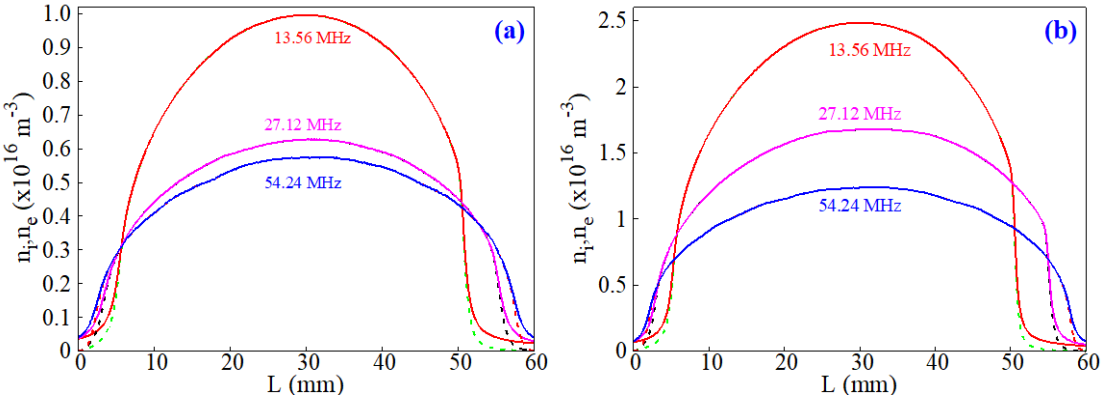


**Figure 2:** The profile of time average ion (solid line) and electron density (dotted line) at different applied frequencies *i.e.* 13.56 MHz, 27.12 MHz and 54.24 MHz for current densities of (a) 50 A/m$^2$ and (b) 100 A/m$^2$.

With increasing driving frequency, the symmetric behavior of the discharge agrees with the results obtained by Bruneau *et al.* [40]. However, in their study the density shows the opposite trend *i.e.* it was increasing with driving frequency. In the present current driven case, the density is decreasing with an increase in driving frequency. At 50 A/m$^2$, the central peak density is 9.96x10$^{15}$ m$^{-3}$ at 13.56 MHz and decreasing to 5.7x10$^{15}$ m$^{-3}$ at 54.24 MHz. Similarly, at 100 A/m$^2$, the central peak density is 2.5x10$^{16}$ m$^{-3}$ at 13.56 MHz and decreasing to 1.24x10$^{16}$ m$^{-3}$ at 54.24 MHz *i.e.* decrease by approximately 50%. Similar kind of decreasing trend is observed in spatially averaged densities. The bulk electron temperature estimated from the Electron Energy Distribution Function (EEDF) [61] is observed to increase from 1.6 eV at 13.56 MHz to 2.3 eV at 54.24 MHz for 50 A/m$^2$, and from 1.65 eV at 13.56 MHz to 2.35 eV at 54.24 MHz for 100 A/m$^2$. We will later show in the manuscript that a decrease in the peak-to-peak discharge voltage and sheath modulation frequency versus driving frequency are responsible for the decreasing trend of the plasma density. For a sinusoidal waveform driven CCP discharge [64], the sheath modulation frequency is dependent on the discharge voltage for a constant driving frequency.

A transition from asymmetric to symmetric and a decrease in plasma density versus driving frequency could also be envisaged by investigating the ionization rate within the discharge system. Figure 3 (a) and 3 (e) shows the time averaged ionization rate for different driving frequencies at 50 A/m$^2$ and 100 A/m$^2$ current density amplitudes respectively. The corresponding time averaged excitation rates for different excited species are shown in figures 3 (b) – 3 (d) and figures 3 (f) – 3 (h). As shown in figure 3, due to longer electron mean free path at lower gas pressure, the ionization and different excitation mechanisms are mostly occurring into the bulk

plasma. The ionization rate (figure 3 (a) and 3 (e)) is higher at 13.56 MHz and decreasing at 54.24 MHz. The corresponding excitation rates to Ar* ($3p^5 4s$), 11.6 eV (figure 3(b) and figure 3(f)), and Ar** ($3p^5 4p$), 13.1 eV (figure 3(c) and figure 3(g)) is also higher at 13.56 MHz and decreasing with a rise in driving frequency. The low energy electrons (~1.5 eV) are further consumed in excitation from Ar* to Ar**, and its rate is highest at 13.56 MHz and decreasing drastically at 54.24 MHz (figure 3(d) and figure 3(h)). This might be attributed to high energy electron beams generated from near to the sheath edge at higher driving frequency, which is responsible for raising the bulk electron temperature through non-linear interaction [63]. Thus, the overall population of low energy electrons responsible for further excitation are reduced. It is further noticed that, as driving frequency increase, the spatial distribution of the ionization rate and different excitation rates becomes symmetric and therefore responsible for the symmetric behavior of the discharge as observed in the plasma density profile shown in figure 2.

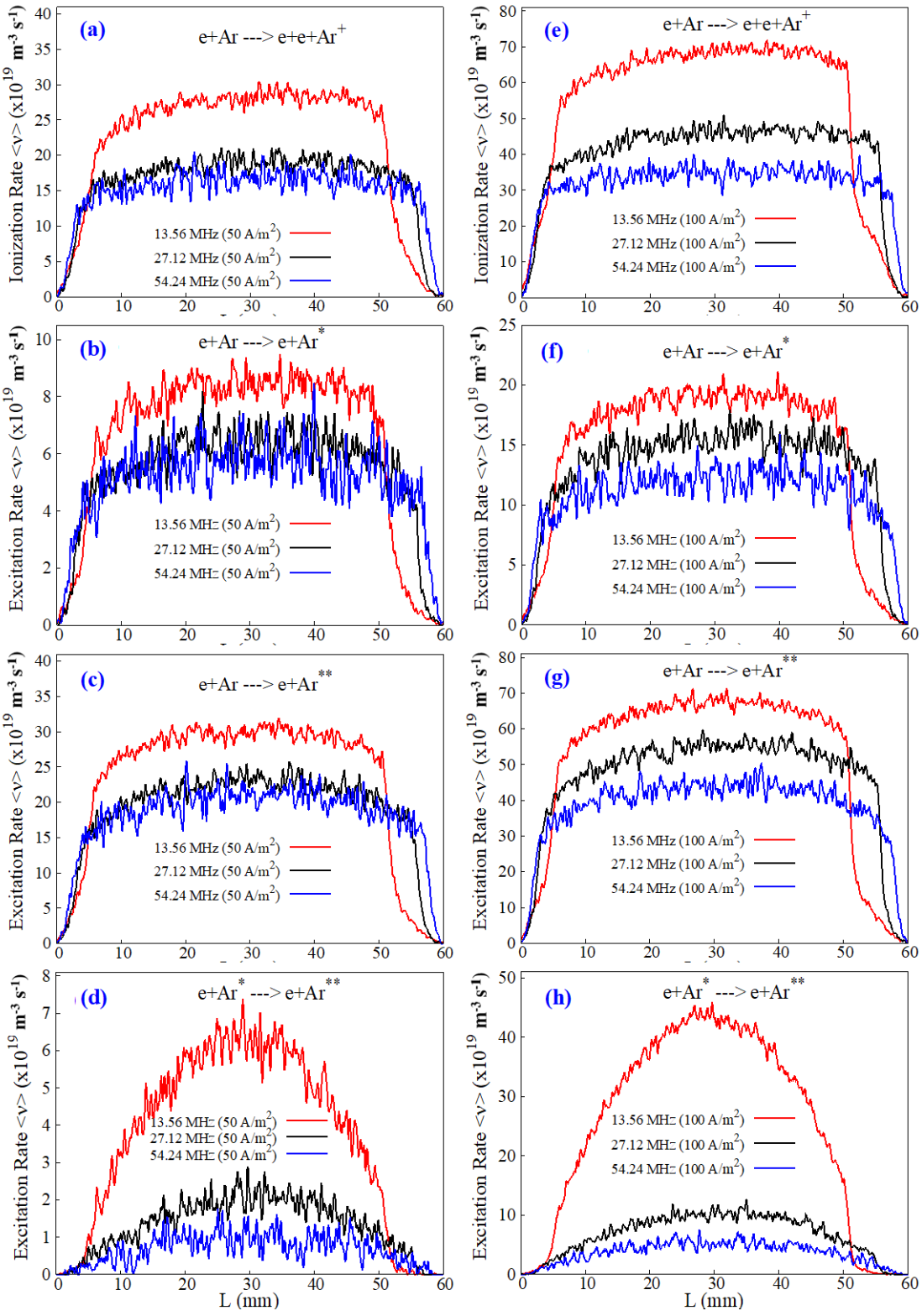


**Figure 3:** Time averaged ionization and excitation rates at different applied frequencies *i.e.* 13.56 MHz, 27.12 MHz and 54.24 MHz: (a) ionization rate, 50 A/m$^2$, (b) Ar* ($3p^5 4s$) excitation rate, 50 A/m$^2$, (c) Ar** ($3p^5 4p$) excitation rate, 50 A/m$^2$, (d) Ar* ($3p^5 4s$) to Ar** ($3p^5 4p$) excitation rate, 50 A/m$^2$, (e) ionization rate, 100 A/m$^2$, (f) Ar* ($3p^5 4s$) excitation rate, 100 A/m$^2$, (g) Ar** ($3p^5 4p$) excitation rate, 100 A/m$^2$, (h) Ar* ($3p^5 4s$) to Ar** ($3p^5 4p$) excitation rate, 100 A/m$^2$.

To further investigate into the ionization mechanism, the spatio-temporal evolutions of ionizing collision rate for different driving frequencies are examined. This is shown in figure 4. The spatio-temporal plots in figure 4 are averaged over last 600 RF cycles. At 50 A/m$^2$ and 13.56 MHz driving frequency (figure 4 (a)), a strong asymmetry is observed in the ionization collision rate *i.e.* it is higher near to grounded electrode when compared to powered electrode and highest during the expanding phase of the sheath. Furthermore, due to nearly collisionless operation the ionization front is penetrating into the bulk plasma and extending up to the opposite sheath. As driving frequency increases to 27.12 MHz, the ionization collision rate asymmetry reduces, and at 54.24 MHz driving frequency it is nearly symmetric. Comparing different driving frequency for same current density *i.e.* either at 50 A/m$^2$ or at 100 A/m$^2$ (figure 4 (a), 4 (b) and 4 (c) or figure 4 (d), 4 (e) and 4 (f)), the ionization collision rate near to the grounded electrode is highest for 13.56 MHz driving frequency. When comparing different current densities, the ionization collision rate is higher at 100 A/m$^2$ current density, however, the effect of increasing driving frequency is similar for both current densities.

At 13.56 MHz, the asymmetric behavior of the ionization rate is attributed to the enhanced pressure (collisionless) heating near to the grounded electrode. As described by the hard wall model [72], one of the factors responsible for enhanced collisionless heating is the sheath velocity. In the present case, we observed that the sheath width is decreasing, however, the sheath velocity is increasing from 4.97x10$^5$ m/s at 13.56 MHz to 5.74x10$^5$ m/s at 54.24 MHz for 50 A/m$^2$. At 100 A/m$^2$, the sheath is 5.44x10$^5$ m/s and 6.4x10$^5$ m/s at 13.56 MHz and 54.24 MHz respectively. This will increase the energy gained by the electrons, and hence ionization collision rate and plasma density should increase. However, we observe an opposite trend *i.e.* the plasma density and ionizing collision rate is decreasing with driving frequency. These suggests that a different phenomenon is responsible here. As shown later in the manuscript, this effect is attributed to a decrease in the discharge voltage versus driving frequency. Further inspecting the spatio-temporal ionization rate, it is noticed that at 13.56 MHz (figure 4 (a) and 4 (d)) multiple beams like ionization collision rate is present near to the expanding sheath edge. The number of multiple ionization beams are higher at higher current density and decrease with driving frequency for both current densities. These multiple beams are caused due to high frequency modulation on the instantaneous sheath edge position and analogue to the sheath modulation in the case of multiple frequency excited CCP discharges [8, 15, 73]. In the following discussion, we further investigate the non-linearity in electric field and discharge voltage to support above fact.

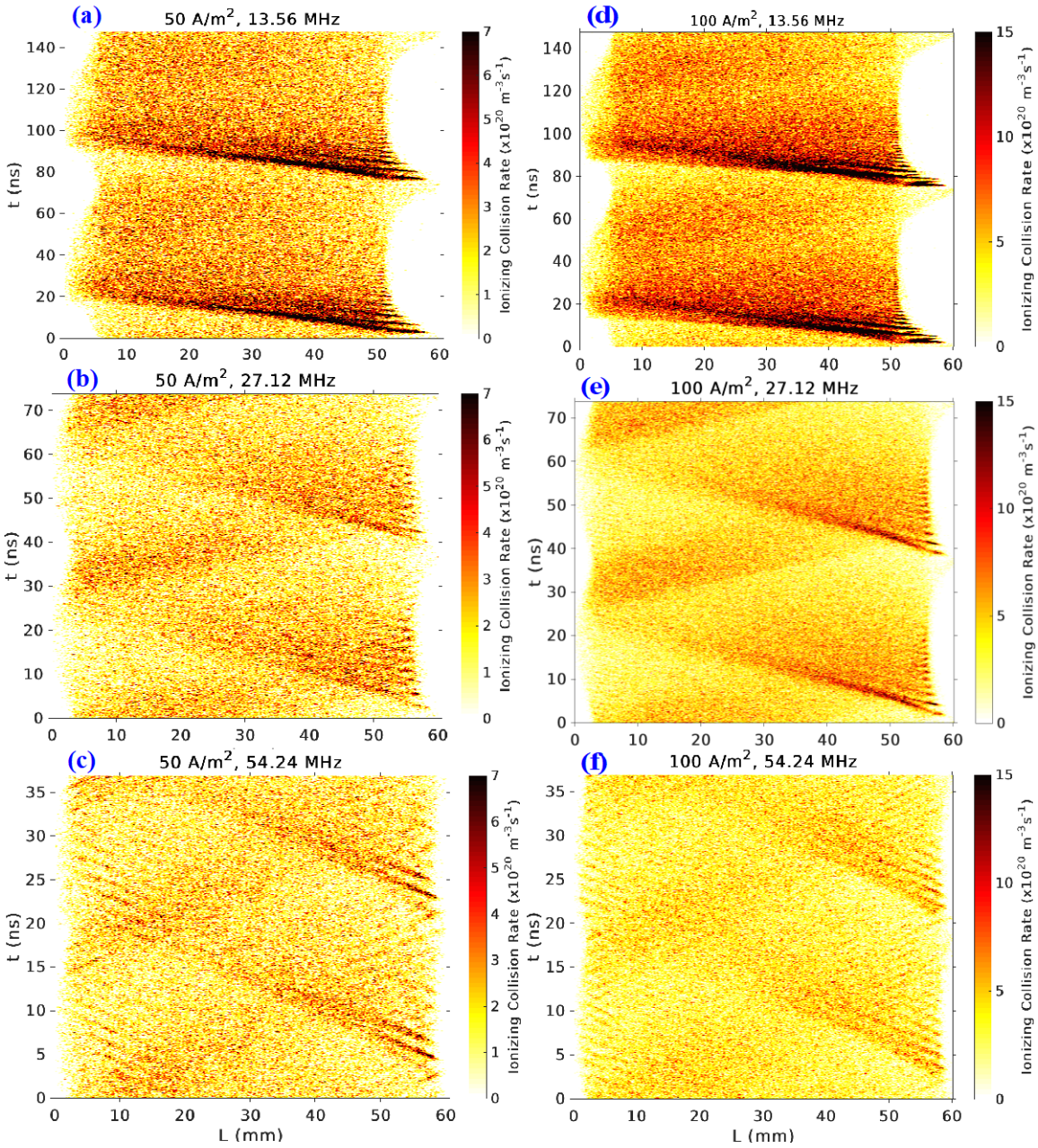


**Figure 4:** Spatio-temporal evolution of ionizing collision rates at different applied frequencies: (a) 13.56 MHz, 50 A/m$^2$, (b) 27.12 MHz, 50 A/m$^2$, (c) 54.24 MHz, 50 A/m$^2$, (d) 13.56 MHz, 100 A/m$^2$, (e) 27.12 MHz, 100 A/m$^2$, and (f) 54.24 MHz, 100 A/m$^2$.

.

To discuss the higher harmonics generation in the discharge, we first investigate the spatio-temporal evolution of electric field in the discharge. This is plotted in figure 5 for different driving frequencies and for current densities of 50 A/m$^2$ and 100 A/m$^2$. The spatio-temporal plots are averaged over last 100 RF cycles when simulation reached to the steady state case. As shown in figure 5 (a) and 5 (d), at 13.56 MHz, the electric field is mostly confined into the sheath region and bulk plasma is almost

quasi-neutral. However, the temporal electric field at the sheath boundary near to the grounded electrode is significantly modified *i.e.* high frequency oscillations are observed on the instantaneous sheath edge position. When the driving frequency increase to 27.12 MHz (figure 5 (b) and 5 (d)), the electric field transients appears in the bulk plasma. The corresponding high frequency oscillation on the temporal electric field near to the grounded electrode is reduced when compared to 13.56 MHz driving frequency. At 54.24 MHz (figure 5 (c) and 5 (e)), the electric field transients are strongest, reaching up to the opposite sheath edge and weakly modifying its instantaneous position. The high frequency oscillations on the grounded temporal electric field is substantially reduced. As discussed earlier, the high frequency modulation on the instantaneous sheath edge position might be responsible for driving higher ionization rate and plasma density in the discharge. As shown in figure 5, the modulation in the spatio-temporal electric field near to the sheath edge is highest at 13.56 MHz and decrease with an increase in the driving frequency. These explains why the ionization rate and plasma density is decreasing with a rise in driving frequency. On the other hand, the energy of the beam is driven by the sheath velocity, which is increasing with driving frequency and therefore one can observe high energy electron beams produced at 54.24 MHz reaching up to the opposite sheath edge. The trend is consistent at both current densities. When comparing the same driving frequencies, for two different current densities, one can observe that the electric field modulation is greater at 100 $A/m^2$. Therefore, the plasma density and ionization rate plotted in figure 2 and figure 3 respectively is higher at 100 $A/m^2$. The corresponding beam energy is also higher at higher current density due to greater sheath width and corresponding sheath velocity. This could be appropriately envisaged at 54.24 MHz (figure 5 (c) and figure 5 (f)), where the high frequency oscillations are higher at 100 $A/m^2$ (figure 5 (f)) when compared to 50 $A/m^2$ (figure 5 (c)). The beam energy at 100 $A/m^2$ (figure 5 (f)) is also higher, therefore, reaching up to the opposite sheath edge and generating the high frequency modulation on the powered electrode sheath. However, the beam energy is lower at 50 $A/m^2$ (figure 5 (c)) *i.e.* it is reaching up to the opposite sheath edge but weakly modifying its instantaneous position. From the results presented in figure 5, it is observed that the high frequency modulation on the sheath edge electric field is responsible for driving higher plasma density in the discharge, whereas, the beam energy is mostly governed by the sheath velocity. At 27.12 MHz (figure 5 (b) and 5 (e)) and 54.24 MHz (figure 5 (c) and 5 (f)), it is further noticed that the electric field transients are not continuous *i.e.* burst like structures are observed. Further, by observing the time-averaged electron heating we will show that this will drive the alternate electron heating and cooling in the bulk plasma.

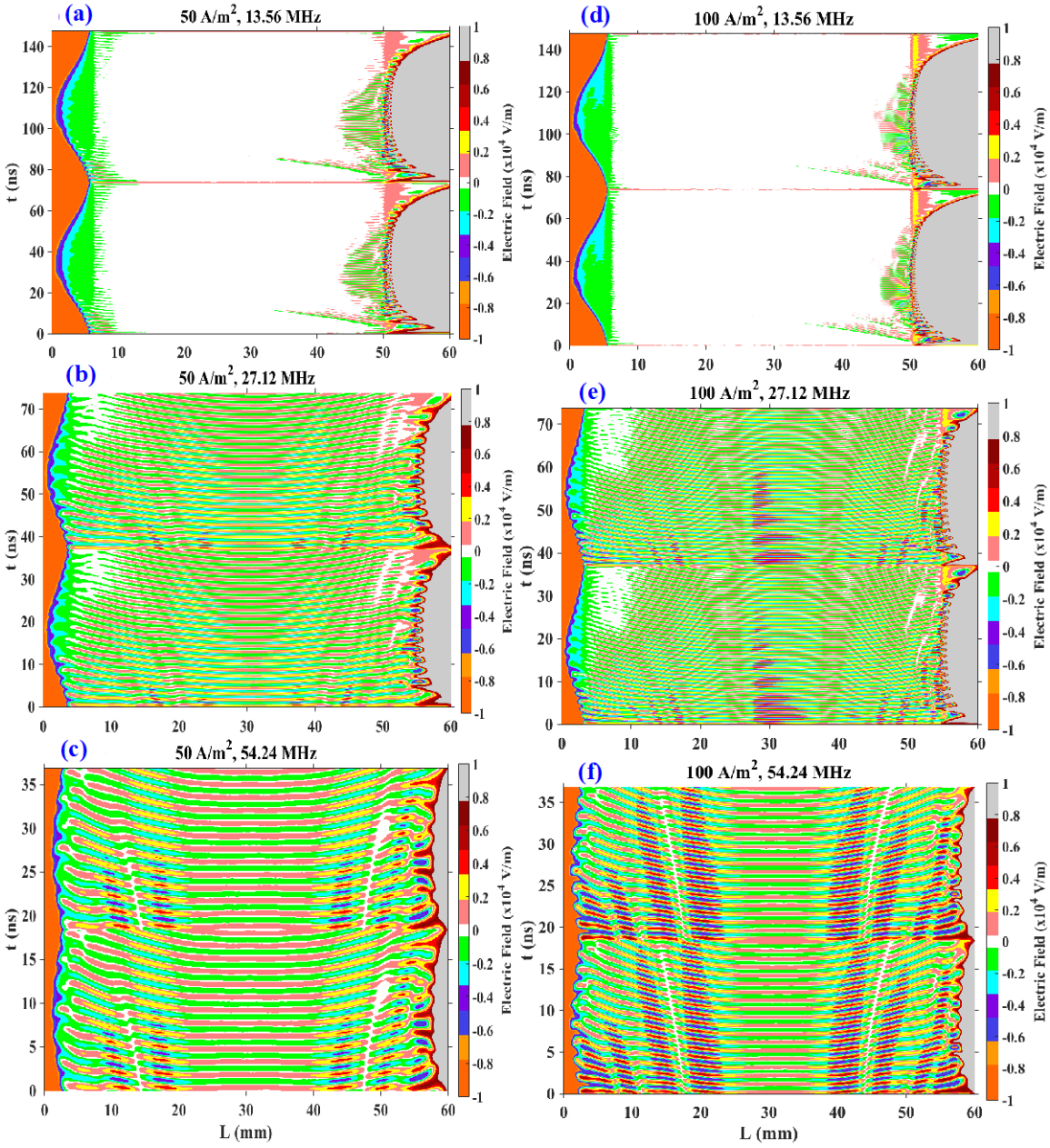


**Figure 5:** Spatio-temporal evolution of electric field at different applied frequencies for 50 A/m$^2$ and 100 A/m$^2$: (a) 13.56 MHz, 50 A/m$^2$, (b) 27.12 MHz, 50 A/m$^2$, (c) 54.24 MHz, 50 A/m$^2$, (d) 13.56 MHz, 100 A/m$^2$, (e) 27.12 MHz, 100 A/m$^2$, and (f) 54.24 MHz, 100 A/m$^2$.

The frequency of instantaneous sheath edge modulation could be deduced by transforming the simulation results from the time domain to the frequency domain. For this purpose, the electric field at the centre of the discharge and peak-to-peak discharge voltage along with its fast fourier transform (FFT) is plotted. This is shown in figure 6 and figure 7 respectively. At 13.56 MHz and 50 A/m$^2$ (figure 6 (a)), 68$^{th}$ (~900 MHz) harmonic is dominantly triggered into the bulk plasma. Several other harmonics are observed up to 650 MHz, but their amplitudes are low *i.e.* below 8%. The 68$^{th}$ harmonic is slightly over electron plasma frequency at the centre of the

discharge, which is ~898 MHz in this case. As driving frequency increase to 27.12 MHz (figure 6 (b)), the frequency of sheath modulation decrease, a distinct $26^{th}$ (~705 MHz) harmonic (dominant frequency) along with its nearby harmonics are observed into the bulk plasma. The frequency of the dominant $26^{th}$ harmonic is slightly higher than electron plasma frequency (~700 MHz) at the centre of the discharge. The amplitude of harmonics observed at 27.12 MHz is higher in comparison to the harmonics observed at 13.56 MHz (figure 6 (a)). At 54.24 MHz (figure 6 (c)), the frequency of sheath modulation is further reduced to 650 MHz ($12^{th}$ harmonic) and several other harmonics are observed (labelled in the figure). The electron plasma frequency is ~650 MHz in this case. At this driving frequency, the amplitude is now distributed over large number of higher harmonics and therefore the amplitude of dominant harmonic ($12^{th}$ harmonics) is lower than the amplitude of dominant harmonic ($26^{th}$ harmonic) observed at 27.12 MHz. Similar results are observed at 100 $A/m^2$ (figure 6 (d), 6 (e) and 6 (f)) *i.e.* the frequency of dominant harmonic is decreasing with an increase in driving frequency and several numbers of higher harmonics are observed at higher driving frequency. Furthermore, for a fixed driving frequency the position of the dominant harmonic is higher at 100 $A/m^2$ in comparison to 50 $A/m^2$. This is due to an increase in the plasma density as current density increases.

Figure 7 shows the corresponding powered electrode voltage and its FFT. The investigation of electrode voltage is useful not only for the further explanation of simulation outcomes but also could be measured experimentally. We first notice that at both current densities the peak-to-peak electrode voltage decreases with an increase in driving frequency *i.e.* from ~865 V to ~190 V at 50 $A/m^2$ and ~1790 V to ~290 V at 100 $A/m^2$. For same driving frequency, the electrode voltage is higher at 100 $A/m^2$ when compared to 50 $A/m^2$ current density. This is attributed to a decrease in the sheath width with driving frequency, which allows higher current to flow through the discharge and therefore electrode voltage drops. We also notice that, at higher driving frequencies, higher harmonics are observed in the electrode voltage that are similar to ones appeared in electric field transients (figure 6). However, the contribution/amplitude of higher harmonics are comparatively lower when compared to higher harmonics in the electric field at the centre of the discharge. At 13.56 MHz (figure 7 (a) and 7 (d)), the FFT shows only fundamental frequency and no higher harmonics are observed. This is due to no electric field penetration (figure 5 (a) and 5 (d)) into the bulk plasma at this driving frequency. The corresponding electric field FFT at the centre of the discharge (figure 6 (a) and 6 (b)) also shows weak presence of higher harmonics. As driving frequency increase to 27.12 MHz (figure 7 (b) and 7 (e)), the fundamental frequency drops and the higher harmonic similar to one observed in the electric field (figure 6 (b) and 6 (e)), *i.e.* $26^{th}$ (~705 MHz) for 50 $A/m^2$ and $43^{rd}$ (~1166 MHz) for 100 $A/m^2$, appears in the discharge voltage. At 54.24 MHz (figure 7 (c) and 7 (f)), the fundamental frequency reduces to below 20% and several higher harmonics are observed with a dominant one at $12^{th}$ harmonic (~650 MHz) for 50 $A/m^2$ and $18^{th}$ (~976 MHz) for 100 $A/m^2$, which is similar to that observed in electric field transients (figure 6 (c) and 6 (f)). These higher harmonics are appeared

due to non-linear interaction of electrons with the oscillating sheath edge responsible for modifying the instantaneous sheath edge positions and generating the multiple electron beams. In contrast to sinusoidal waveform driven CCP discharges [74], a current driven CCP excited by saw-tooth waveform could generate higher harmonics in the electrode voltage. This is due to several harmonics composed in the applied current waveform. In the previous study of sinusoidal case [74], it was noticed that a strong electric field reversal is created at an instant after the beam acceleration and thereafter attracts bulk electrons for further acceleration. For saw-tooth like waveform, the sheath edge expansion is much faster in comparison to sinusoidal case and therefore one could expect greater energy transfer and therefore higher energetic electrons acceleration.

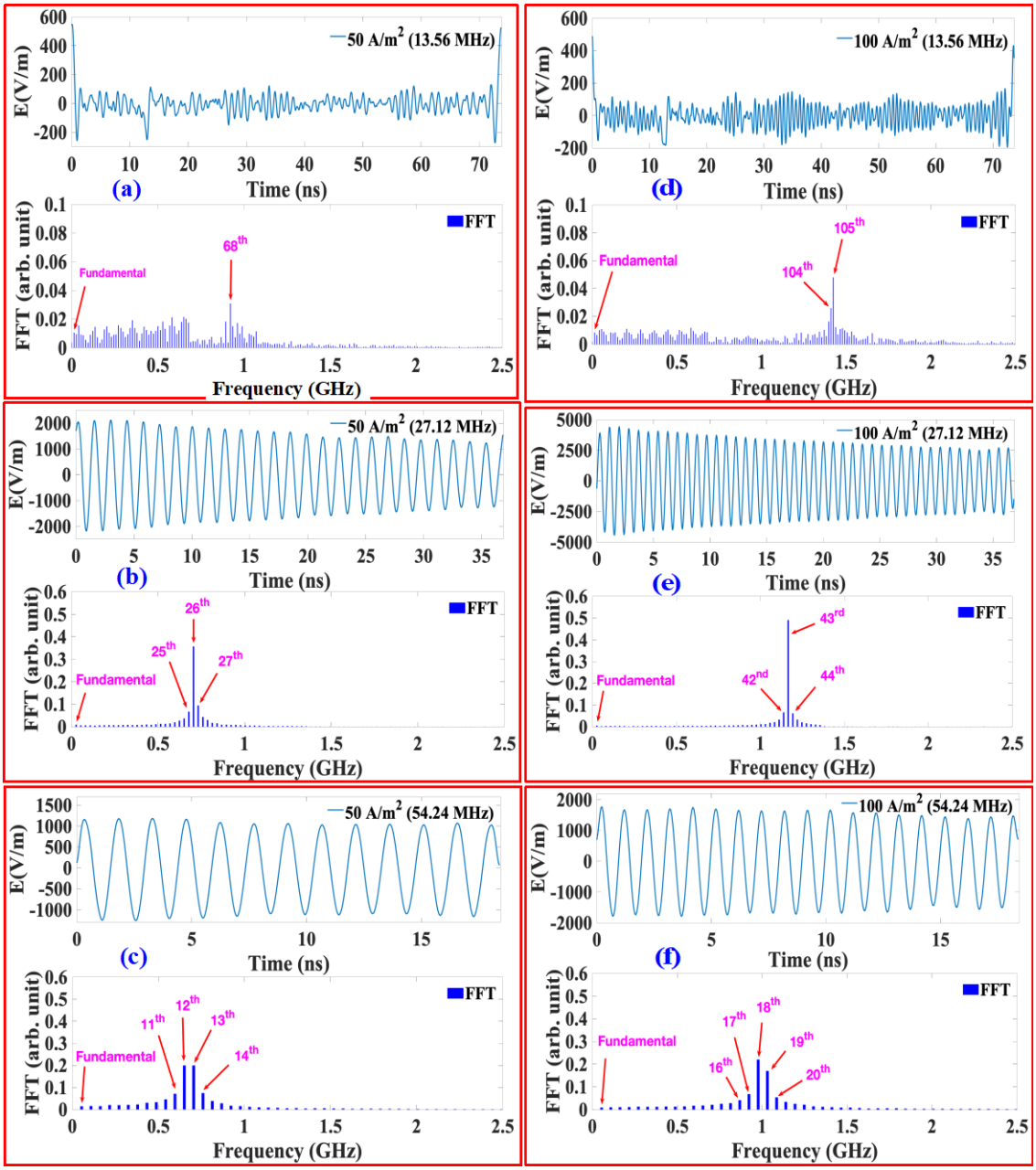

**Figure 6:** Evolution of electric field with time and its FFT at the centre of the discharge for different applied frequencies: (a) 13.56 MHz, 50 A/m$^2$, (b) 27.12 MHz, 50 A/m$^2$, (c) 54.24 MHz, 50 A/m$^2$, (d) 13.56 MHz, 100 A/m$^2$, (e) 27.12 MHz, 100 A/m$^2$, and (f) 54.24 MHz, 100 A/m$^2$.

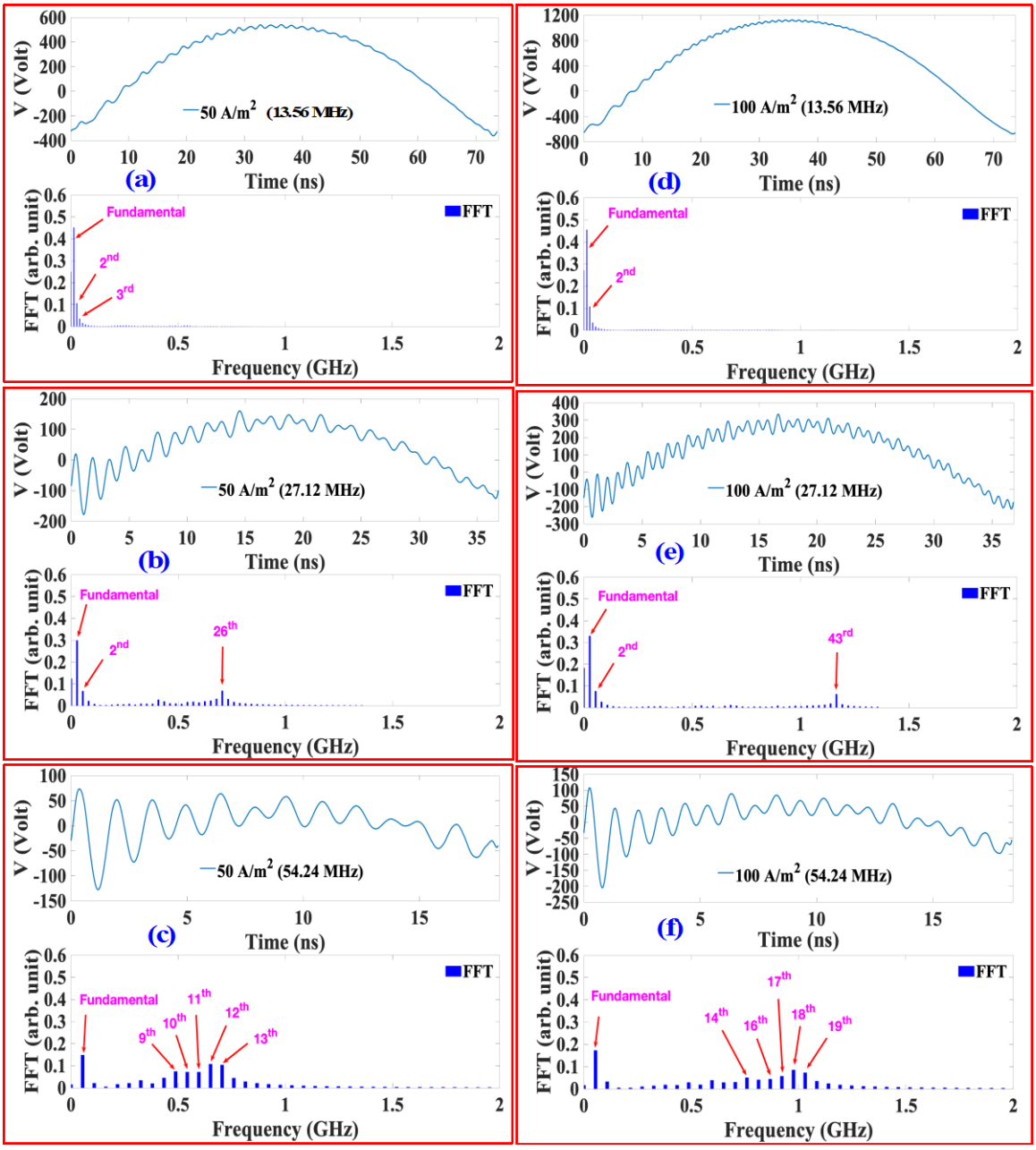


**Figure 7:** Evolution of electrode voltage with time and its FFT for different applied frequencies: (a) 13.56 MHz, 50 A/m$^2$, (b) 27.12 MHz, 50 A/m$^2$, (c) 54.24 MHz, 50 A/m$^2$, (d) 13.56 MHz, 100 A/m$^2$, (e) 27.12 MHz, 100 A/m$^2$, and (f) 54.24 MHz, 100 A/m$^2$.

We next present the phase-averaged electron heating in the discharge. This is shown in figure 8. For both current densities, an asymmetry is observed in the phase-averaged electron heating *i.e.* it is higher near to the grounded sheath when compared to the powered electrode. The difference between energy losses at the powered electrode and grounded is decreasing with driving frequency suggesting that the discharge is becoming nearly symmetric at higher driving frequencies. When comparing different driving frequencies at 50 A/m$^2$ current density, the electron heating near to the grounded sheath is decreasing from ~100 W/m$^2$ at 13.56 MHz to ~15 W/m$^2$ at 54.24 MHz driving frequency. At 13.56 MHz, the heating in maximum near to the sheath edge followed by electron cooling in the bulk plasma. A strong negative <*J.E*> is observed near to the sheath edge, which is due to the reflected high energy electrons interacting with the bulk plasma causing net cooling in this region [75]. At 27.12 MHz and 54.24 MHz, the electron heating is further propagating the bulk plasma. An alternate electron heating and cooling *i.e.* beats like structure are observed up to the centre of the discharge. This is a further evidence of multiple burst of high energy electrons. These high-energy electrons bursts produced from near to the expanding sheath edge travel through the bulk plasma and produces positive and negative space charge/electric field in the spatial directions as observed in the spatio-temporal electric field plotted in figures 5 (b), 5 (c), 5 (e) and 5 (f). Since the current must be conserved, the alternated sign of electric field generates positive and negative heating in the bulk plasma. As shown in the inset figures 8 (a) and 8 (b), the corresponding amplitude is higher at 54.24 MHz when compared to 27.17 MHz. This is due to the faster sheath expansion at 54.24 MHz that drives more energetic electron bursts in comparison to 27.12 MHz and therefore one might expect to see an increase in the amplitude of electron heating and cooling at higher driving frequency. Similar trend is observed at a current density of 100 A/m$^2$, except, the phase-averaged electron heating in higher and the amplitude of alternate positive and negative heating is greater in comparison to 50 A/m$^2$. The above results suggest that due to high frequency modulation and multiple bursts like high energy electrons, the heating in these discharges will not be described accurately by simple analytical models.

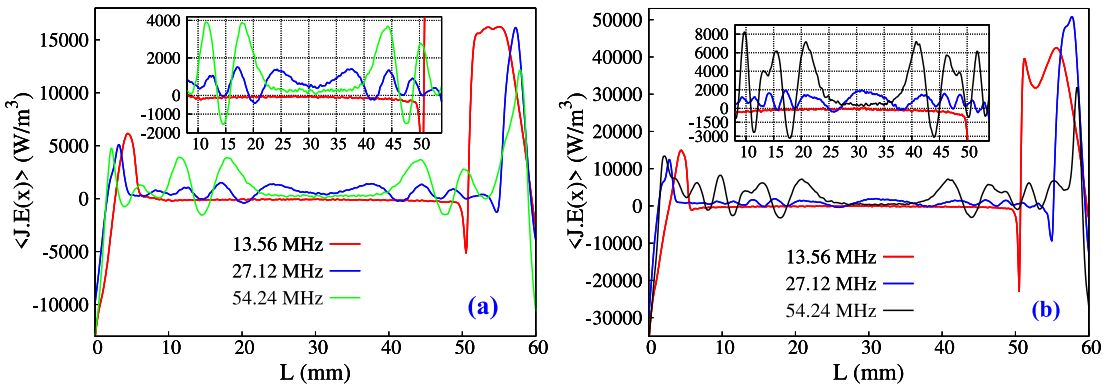

**Figure 8:** Time average electron heating (<J.E>) in the discharge at different applied frequencies *i.e.* 13.56 MHz, 27.12 MHz and 54.24 MHz for current densities of (a) 50 $A/m^2$ and (b) 100 $A/m^2$.

## 4. Summary and Conclusion

The effect of driving frequency on discharge asymmetry, electric field/voltage non-linearity and electron heating mechanisms of a low pressure (5 mTorr) capacitively coupled argon plasma discharge excited by sawtooth like current waveform is investigated using particle-in-cell (PIC)/Monte Carlo Collisions (MCC) simulation. For a constant current density, the plasma density is highest at lower driving frequency and discharge is highly asymmetric. As driving frequency increase, the plasma density along with the ionization rate and excitation rate decrease, and their profiles become nearly symmetric. Multiple ionization beams are observed from near to the expanding phase of the sheath edge at the grounded electrode. These multiple ionization beams are extending up to the opposite sheath edge and, are their numbers higher and dense at lower driving frequency and becoming lower in numbers and less dense with a further rise in driving frequency.

An investigation of the spatio-temporal electric field shows high frequency modulation on the instantaneous sheath edge position at the grounded electrode. The frequency of sheath modulation is highest at lower driving frequency and therefore drive enhanced plasma density and lower electron temperature in the discharge. As driving frequency increase, the frequency of sheath modulation decreases and the transients are more energetic due to higher sheath velocity, reaching up to the opposite sheath edge and modifying its instantaneous position. The Fourier spectrum of electric field at the centre of the discharge confirms the presence of higher harmonics corresponds to the high frequency sheath modulation. Similar non-linearities/higher harmonics are generated on the voltage waveform at the powered electrode. The simulation results are consistent at different current densities. Therefore, it is concluded that the high frequency oscillations drive plasma density and the sheath velocity drive energetic electric field transients in the discharge.

The phase-averaged electron heating near to the sheath edge at both electrodes decreases with an increase in driving frequency. An enhanced high frequency modulation on the grounded sheath at lower driving frequency is responsible for greater phase-averaged electron heating. The spatial distribution of electron heating shows that at lower driving frequency, the phase-averaged electron heating is maximum near to the sheath edge followed by electron cooling in the bulk plasma. However, at higher driving frequencies, along with the electron heating near to the sheath edge, alternate electron heating and cooling is observed in the bulk plasma. The amplitude of such heating and cooling is higher at 54.24 MHz when compared to 27.12 MHz and attributed to spatial positive and negative electric field/charge

separation caused by the bursts of high energy electrons produced from near to the sheath edge.

## References


[1] Lieberman M and Lichtenberg A J, *Principles of Plasma Discharges and Materials Processing* (Wiley: NJ, 2005)

[2] Goto H H, Lowe H D and Ohmi T 1992 *J. Vac. Sci. Technol. A* **10** 3048

[3] Boyle P C, Ellingboe A R and Turner M M 2004 *Plasma Sources Sci. Technol. 13* 493

[4] Kitajima T, Takeo Y, Petrovi´c Z Lj and Makabe T 2000 *Appl. Phys. Lett.* **77** 489

[5] Sharma S and Turner M M 2013 *Journal of Physics D: Applied Physics* **46** 285203

[6] Lee J K, Manuilenko O V, Babaeva N Yu, Kim H C and Shon J W 2005 *Plasma Sources Sci. Technol.* **14** 89

[7] Kawamura E, Lieberman M A and Lichtenberg A J 2006 *Phys. Plasmas* **13** 053506

[8] Sharma S and Turner M M 2014 *Journal of Physics D: Applied Physics* **47** 285201

[9] Derzsi A, Schuengel E, Donko Z and Schulze J 2015 *Open Chem.* **13** 346

[10] Gibson A R, Greb A, Graham, W G and Gans T 2015 *Appl. Phys. Lett.* **106** 054102

[11] Wu Alan C F, Lieberman M A and Verboncoeur J P 2007 *J. Appl. Phys.* **101** 056105

[12] Kim H C and Lee J K 2004 *Phys. Rev. Lett.* **93** 085003

[13] Kim H C, Iza F, Yang S S, Radmilovic-Radjenovic M and Lee J K 2005 *J. Phys. D: Appl. Phys.* **38** R283

[14] Park G Y, You S J, Iza F and Lee J K 2007 *Phys. Rev. Lett.* **98** 085003

[15] Sharma S, Mishra S K, Kaw P K and Turner M M 2017 *Phys. plasmas* **24** 013509

[16] Heil B G, Schulze J, Mussenbrock T, Brinkmann R P and Czarnetzki U 2008 *IEEE Trans. Plasma Sci.* **36** 1404

[17] Heil B G, Czarnetzki U, Brinkmann R P and Mussenbrock T 2008 *J. Phys. D: Appl. Phys.* **41** 165202

[18] Donko Z, Schulze J, Heil B G and Czarnetzki U 2009 *J. Phys. D: Appl. Phys.* **42** 025205

[19] Zhang Q-Z, Jiang W, Hou L-J and Wang Y-N 2011 *J. Appl. Phys.* **109** 013308

[20] Korolov I, Donk´o Z, Czarnetzki U and Schulze J 2012 *J. Phys. D Appl. Phys.* **45** 465205

[21] Bora B, Bhuyan H, Favre M, Wyndham E and Wong C S 2013 *J. Appl. Phys.* **113** 153301

[22] Lafleur T and Booth J P 2013 *Appl. Phys. Lett.* **102** 154104

[23] Coburn J W and Kay E 1972 *J. Appl. Phys.* **43** 4965

[24] Köhler K, Coburn J W, Horne D E, Kay E and Keller H 1985 *J. Appl. Phys.* **57** 59
[25] Lieberman M A and Savas S E 1990 *J. Vac. Sci. Technol. A* **8** 1632
[26] Lafleur T, Chabert P and Booth J P 2013 *J. Phys. D: Appl. Phys.* **46** 135201
[27] Lafleur T 2016 *Plasma Sources Sci. Technol.* **25** 013001
[28] Wang S-B and Wendt A E 2000 *J. Appl. Phys.* **88** 643
[29] Patterson M M, Chu H Y and Wendt A E 2007 *Plasma Sources Sci. Technol.* **16** 257
[30] Schulze J, Schuengel E, Czarnetzki U and Donko Z 2009 *J. Appl. Phys.* **106** 063307
[31] Baloniak T, Reuter R and Keudell A V 2010 *J. Phys. D: Appl. Phys.* **43** 335201
[32] Schulze J, Schuengel E, Donk´o Z and Czarnetzki U 2011 *Plasma Sources Sci. Technol.* **20** 015017
[33] Sharma S, Mishra S K, Kaw P K, Das A, Sirse N and Turner M M 2015 *Plasma Sources Sci. Technol.* **24** 025037
[34] Schungel E, Donko Z, Hartmann P, Derzsi A, Korolov I and Schulze J 2015 *Plasma Sources Sci. Technol.* **24**, 045013
[35] Zhang Y, Kushner M J, Sriraman S, Marakhtanov A, Holland A and Paterson A 2015 *J. Vacuum Science & Technology A* **33** 031302
[36] Wang J K and Johnson E V 2017 *Plasma Sources Sci. Technol.* **26** 01LT01
[37] Hrunski D, Mootz F, Zeuner A, Janssen A, Rost H, Beckmann R, Binder S, Schuengel E, Mohr S, Luggenh¨olscher D, Czarnetzki U and Grabosch G 2013 *Vacuum* **87** 114
[38] Schuengel E, Hofmann R, Mohr S, Schulze J, Ropcke J and Czarnetzki U 2015 *Thin Solid Films* **574** 60
[39] Bruneau B, Novikova T, Lafleur T, Booth J P and Johnson E V 2014 *Plasma Sources Sci. Technol.* **23** 065010
[40] Bruneau B, Novikova T, Lafleur T, Booth J P and Johnson E V 2015 *Plasma Sources Sci. Technol.* **24** 015021
[41] Bruneau B, Gans T, O'Connell D, Greb A, Johnson E V and Booth J P 2015 *Physical Review Letters* **114** 125002
[42] Donko Z, Schulze J, Heil B G and Czarnetzki U 2009 *J. Phys. D: Appl. Phys.* **42** 025205
[43] Schulze J, Schuengel E and Czarnetzki U 2009 *J. Phys. D: Appl. Phys.* **42** 092005
[44] Schuengel E, Zhang Q-Z, Iwashita S, Schulze J, Hou L-J, Wang Y-N and Czarnetzki U 2011 *J. Phys. D: Appl. Phys.* **44** 285205
[45] Schuengel E, Mohr S, Schulze J and Czarnetzki U 2015 *Appl. Phys. Lett.* **106** 054108
[46] Schulze J, Schuengel E, Donko Z and Czarnetzki U 2011 *Plasma Souces Sci. Technol.* **20** 015017
[47] Zhang Y, Zafar A, Coumou D, Shannon S and Kushner M 2015 *J. Appl. Phys.* **117** 233302
[48] Lafleur T, Delattre P A, Johnson E V and Booth J P 2012 *Appl. Phys. Lett.* **101**

124104
[49] Derzsi A, Korolov I, Schuengel E, Donko Z and Schulze J 2013 *Plasma Souces Sci. Technol.* **22** 065009
[50] Diomede P, Economou D J, Lafleur T, Booth J P and Longo S 2014 *Plasma Souces Sci. Technol.* **23** 06504
[51] Bruneau B, Lafleur T, Booth J P and Johnson Erik 2016 *Plasma Sources Sci. Technol.* **25** 025006
[52] Turner M M, and Chabert P 2014 *Appl. Phys. Lett.* **104** 164102
[53] Turner M M, and Chabert P 2017 *J. Phys. D: Appl. Phys* **50** 23LT02
[54] Hockney R W and Eastwood J W 1988 *Computer simulation using particles Adam Hilger, Bristol*
[55] Birdsall C K 1991 *Plasma physics via computer simulation Adam Hilger, Bristol*
[56] Turner M M, Hutchinson A W, Doyle R A and Hopkins M B 1996 *Phys. Rev. Lett.* **76** 2069
[57] Boyle P C, Ellingboe A R and Turner M M 2004 *Plasma Sources Sci. Technol.* **13** 493
[58] Lauro-Taroni L, Turner M M and Braithwaite N St J 2004 *J. Phys. D: Appl. Phys.* **37** 2216
[59] Turner M M 2013 *Plasma Sources Sci. Technol.* **22** 055001
[60] Conway J, Kechkar S, O Connor N, Gaman C, Turner M M and Daniels S 2013 *Plasma Sources Sci. Technol.* **22** 045004
[61] Sharma S, Sirse N, Kaw P K, Turner M M and Ellingboe A R 2016 *Phys. Plasmas* **23** 110701
[62] Sharma S, Sen A, Sirse N, Turner M M and Ellingboe A R 2018 *Physics of Plasmas* **25,** 080705
[63] Sharma S, Sirse N, Turner M M and Ellingboe A R 2018 *Physics of Plasmas* **25,** 063501
[64] Sharma Sarveshwar, Sirse N, Sen A, Wu J S, and Turner M M 2019 *J. Phys. D: Appl. Phys.* **52** 365201
[65] Sharma S, Sirse N, Sen A, Turner M M and Ellingboe A R 2019 *Physics of Plasmas* **26** 103508
[66] Sharma S, Sirse N, Kuley A and Turner M M 2020 *Plasma Sources Sci. and Technol.* **29** 045003
[67] Verboncoeur J P 2005 *Plasma Phys. Control. Fusion* **47** A231
[68] Turner M M, Derzsi A, Donko Z, Eremin D, Kelly S J, Lafleur T and Mussenbrock T 2013 *Phys. Plasmas* **20** 013507
[69] Shahid R and Kushner Mark J 1997 *J. Appl. Phys.* **82** 2805
[70] Godyak V A 1986 Soviet Radio Frequency Discharge Research (Delphic: Falls Church, VA)
[71] Qiu W D, Bowers K J and Birdsall C K 2003 *Plasma Sources Sci. Technol.* **12** 57
[72] Godyak V A 1972 *Sov. Phys.—Tech. Phys.* **16** 1073
[73] Sharma S and Turner M M 2013 *J. Phys. D: Appl. Phys* **46** 285203

[74] Wilczek S, Trieschmann J, Schulze J, Donko Z, Brinkmann R P and Mussenbrock T 2018 *Plasma Sources Sci. Technol.* **27** 125010
[75] Kaganovich I D, Polomarov O V and Theodosiou C E 2006 *IEEE Trans. Plasma Sci.* **34** 696